Korean Journal of Remote Sensing, Vol.25, No.3, 2009, pp.255~261

# New Unsupervised Classification Technique for Polarimetric SAR Images

**Yisok Oh †, Kyung-Yup Lee, and Geba Jang**

Department of Electronic Information and Communication Engineering, Hongik University, Seoul, Korea

**Abstract :** A new polarimetric SAR image classification technique based on the degree of polarization (DoP) and the co-polarized phase-difference (CPD) is presented in this paper. Since the DoP and the CPD of a scattered wave provide information on the randomness of the scattering and the type of scattering mechanisms, at first, the statistics of the DoP and CPD are examined with measured polarimetric SAR image data. Then, a DoP-CPD diagram with appropriate boundaries between six different classes is developed based on the SAR image. The classification technique is verified using the JPL AirSAR and ALOS PALSAR polarimetric data. The technique may have capability to classify an SAR image into six major classes; a bare surface, a village, a crown-layer short vegetation canopy, a trunk-layer short vegetation canopy, a crown-layer forest, and a trunk-dominated forest.

Key Words : SAR image classification technique, degree of polarization, co-polarized phase difference.

## 1. Introduction

SAR (synthetic aperture radar) has the capability to image Earth in both day and night, and for almost all weather conditions. Nowadays, many space-borne and airborne polarimetric SAR systems are available (Boerner, 2003). The SAR uses signal processing to synthesize a high spatial resolution image of the earth's surface reflectivity. There are various supervised and unsupervised classification algorithms for polarimetric SAR images (Ulaby and Elachi, 1990; Lee and Pottier, 2009) such as the maximum likelihood method (Kong *et al*., 1988) and minimum distance classifier based on the Wishart distribution (Lee *et al*., 1994), the decomposition technique (Van zyl, 1989), and the entropy/alpha technique (Cloude and Pottier, 1997). The most common unsupervised technique for polarimetric SAR images is the entropy/alpha-based classification technique. The entropy/alpha-based technique is to classify the polarimetric response of each pixel into an entropy-alpha diagram, in which the entropy and alpha are computed from Eigen analysis of the covariance matrices. Although the Eigen analysis may be an excellent technique to analyze an information matrix, it has some weak points for the SAR image classification. In the process of the Eigen analysis, the magnitudes of the covariance matrix elements are

Received June 10, 2009; Revised June 30, 2009; Accepted July 1, 2009.

† Corresponding Author: Yisok Oh (yisokoh@hongik.ac.kr)

normalized such that the information in the magnitudes is lost, and consequently it prevents us to proceed to the decomposition process after the Eigen analysis. In this paper, we propose one unsupervised classification technique using the degree of polarization (DoP) and the co-polarized phase-difference (CPD) statistics (Ulaby, *et al*., 1992). It is shown that the DoP is closely related to the entropy, and the CPD to the alpha angle. A DoP-CPD diagram is proposed for classifying any polarimetric SAR image data. The new classification technique is verified with polarimetric PALSAR image data. This classification technique does not include any normalization process for the magnitudes of the covariance matrices.

## 2. Degree of Polarization and Phased Difference

The DoP is defined as the relation of the Stokes parameters, which can be computed from the measured Stokes scattering operator matrix or the covariance matrix. The DoP of a scattered wave provides information on the randomness of the scattering from natural targets (Rio, *et al*., 2006), because the DoP depends on the effect of multiple reflections. For full-polarized waves, the scattered electric field is related with the incident wave with the scattering matrix.

The complex scattering matrix $\overline{\overline{S}}$ is defined as in (Sinclair, 1950).

$$\begin{pmatrix} E_h^s \\ E_v^s \end{pmatrix} = \frac{e^{-jk_0 r}}{r} \begin{pmatrix} S_{hh} & S_{hv} \\ S_{vh} & S_{vv} \end{pmatrix} \begin{pmatrix} E_h^i \\ E_v^i \end{pmatrix} \tag{1}$$

The Stokes vector for a polarized wave are defined as

$$\overline{F^s} = \begin{bmatrix} I^s \\ Q^s \\ U^s \\ V^s \end{bmatrix} == \begin{bmatrix} \langle |E_h^s|^2 \rangle + \langle |E_v^s|^2 \rangle \\ \langle |E_h^s|^2 \rangle - \langle |E_v^s|^2 \rangle \\ \langle 2\mathrm{Re}(E_h^s E_v^{s*}) \rangle \\ \langle 2\mathrm{Im}(E_h^s E_v^{s*}) \rangle \end{bmatrix} \tag{2}$$

where <⋯> indicates the ensemble average (Ulaby and Elachi, 1990). For general cases, a partially polarized wave has the following relation:

$$I^{s2} \geq Q^{s2} + U^{s2} + V^{s2} \tag{3}$$

The DoP of the partially polarized wave is defined as in (Ulaby and Elachi, 1990).

$$DoP = \frac{Q^{s2} + U^{s2} + V^{s2}}{I^{s2}} \tag{4}$$

One form of the covariance matrix $\overline{\overline{C}}$ and its elements are shown in terms of the elements of the scattering matrix $\overline{\overline{S}}$ as follows:

$$\langle [C] \rangle = \langle k_L k_L^{*t} \rangle = \frac{1}{N} \sum_{i=1}^{N} \vec{k_L}(i) \bullet \vec{k_L}(i)^{*T} = \frac{1}{N} \sum_{i=1}^{N} C_i \tag{5}$$

$$\text{where} \quad k_L = [S_{HH} \quad 2S_{HV} \quad S_{VV}]^T$$

$$\langle [C] \rangle = \begin{bmatrix} \langle S_{HH} S_{HH}^* \rangle & \sqrt{2}\langle S_{HH} S_{HV}^* \rangle & \langle S_{HH} S_{VV}^* \rangle \\ \sqrt{2}\langle S_{HV} S_{HH}^* \rangle & 2\langle S_{HV} S_{HV}^* \rangle & \sqrt{2}\langle S_{HV} S_{VV}^* \rangle \\ \langle S_{VV} S_{HH}^* \rangle & \sqrt{2}\langle S_{VV} S_{HV}^* \rangle & \langle S_{VV} S_{VV}^* \rangle \end{bmatrix} \tag{6}$$

For an h-polarized wave incidence ($E_v^i = 0$), the received Stokes parameters are expressed with the normalization of $|E_h^i| = 1$.

$$\begin{aligned} I_h^s &= \frac{1}{r^2}\left\{\langle C_{11} \rangle + \frac{1}{2}\langle C_{22} \rangle\right\} \\ Q_h^s &= \frac{1}{r^2}\left\{\langle C_{11} \rangle - \frac{1}{2}\langle C_{22} \rangle\right\} \\ U_h^s &= \frac{1}{r^2}\left\{\sqrt{2}\mathrm{Re}(\langle C_{12} \rangle)\right\} \\ V_h^s &= \frac{1}{r^2}\left\{\sqrt{2}\mathrm{Im}(\langle C_{12} \rangle)\right\} \end{aligned} \tag{7}$$

For a *v*-polarized wave incidence ($E_h^i = 0$), the received Stokes parameters are expressed with the normalization of $|E_v^i| = 1$.

$$\begin{aligned} I_v^s &= \frac{1}{r^2}\left\{\langle C_{33} \rangle + \frac{1}{2}\langle C_{22} \rangle\right\} \\ Q_v^s &= \frac{1}{r^2}\left\{\langle C_{33} \rangle - \frac{1}{2}\langle C_{22} \rangle\right\} \\ U_v^s &= \frac{1}{r^2}\left\{\sqrt{2}\mathrm{Re}(\langle C_{23} \rangle)\right\} \\ V_v^s &= \frac{1}{r^2}\left\{\sqrt{2}\mathrm{Im}(\langle C_{23} \rangle)\right\} \end{aligned} \tag{8}$$

The DoP is computed by averaging the DoP for *h*- and *v*-polarized wave incidence,

$$DoP = \frac{DoP_h + DoP_v}{2} \tag{9}$$

The DoP explains the feature how much the effect of multiple reflections is contained (Elices and Le Jeune, 1997). Hence, the DoP could be used as an important factor for classifying classes. For example, the bare surface or buildings have high values of the DoP because there are only simple reflections, while the forest or pastures have low values of the DoP because it contains various multiple reflections effect.

The CPD is defined as the ensemble average of the phase difference between the *hh*- and *vv*-polarized scattered waves. In the backscattering case, the measured scattering matrix by a polarimetric radar system consists of five quantities; $|S_{hh}|$, $|S_{vv}|$ and $|S_{hv}|$, $\Phi_c=\Phi_{hh}-\Phi_{vv}$, and $\Phi_x=\Phi_{hv}-\Phi_{vv}$. The scattering matrix $S$ can be written as

$$S = e^{-i\phi_{vv}} \begin{pmatrix} |S_{hh}|\, e^{-i\phi_c} & |S_{hv}|\, e^{-i\phi_x} \\ |S_{vh}|\, e^{-i\phi_x} & |S_{vv}| \end{pmatrix} \tag{10}$$

The CPD $\Phi_c$ can be written as

$$\phi_c = \phi_{hh} - \phi_{vv} = \tan^{-1}\left(\frac{\langle \mathrm{Im}(S_{hh}S_{vv}^*)\rangle}{\langle \mathrm{Re}(S_{hh}S_{vv}^*)\rangle}\right) = \tan^{-1}\left(\frac{\langle \mathrm{Im}(C_{13})\rangle}{\langle \mathrm{Re}(C_{13})\rangle}\right) \tag{11}$$

The cross-polarized phase difference (XPD) $\Phi_x$ can be written as

$$\phi_x = \phi_{hv} - \phi_{vv} = \tan^{-1}\left(\frac{\langle \mathrm{Im}(S_{hv}S_{vv}^*)\rangle}{\langle \mathrm{Re}(S_{hv}S_{vv}^*)\rangle}\right) = \tan^{-1}\left(\frac{\langle \mathrm{Im}(C_{23})\rangle}{\langle \mathrm{Re}(C_{23})\rangle}\right) \tag{13}$$

For most natural targets, the cross-polarized phase angle $\Phi_x$ is uniformly distributed over $[0, 2\pi]$, and therefore, contains less target-specific information. On the other hand, the CPD $\Phi_c$ shows a Gaussian PDF with the standard deviation and the mean values which depend on the target characteristics. Hence, the CPD contains some target specific information (Ulaby, *et al*., 1990). For extreme cases, for example, CPD=0˚ for radar scattering from a flat surface, and CPD=180˚ for a dihedral-type scattering. Otherwise, the CPD has various values depending on the scattering mechanisms, such as single-bounce scattering, double bounce scattering and volume scattering. Hence, the feature of $\Phi_c$ has good information for classifying polarimetric SAR data.

## 3. DoP-CPD Diagram

The bare surface or buildings have high values of the DoP because almost reflection is not complex, while the forest or pastures have low values of the DoP because it contains various multiple reflections effect. Otherwise, the CPD has various values depending on the scattering mechanisms, such as single-bounce scattering, double bounce scattering and volume scattering. For example, CPD=0˚ for radar scattering from a flat surface, and CPD=180˚ for a dihedral-type scattering.

Polarimetric SAR image scenes for several sites in Korea could be obtained from the PACRIM-II campaign using the JPL AirSAR system in September, 2000, at P-, L- and C-bands. Among these polarimetric AirSAR images, we selected an image of a study area near Busan in Korea, because the study area includes many different types of terrains. The polarimetric SAR image, at first, is filtered using the Lee filter for a better accuracy. Then, we selected four different sample areas in the study site; *i.e*., a bare surface, a short vegetation field, a forest, and a town area. Size of each sample area was selected such that it has more than 1200 pixels.

The DoP and CPD values of each pixel of a sample

area are positioned in the DoP-CPD diagram with the vertical axis of the DoP and the horizontal axis of the CPD. Histograms for the DoP and the CPD distributions are also attached on the DoP-CPD diagram for a better visual aid. Fig. 1 shows the DoP-CPD diagram for a bare surface which is a relatively smooth foreshore, while Figs. 2, 3 and 4 show the DoP-CPD diagrams for a village area, a short vegetation area, and a tall vegetation area, respectively.

The PDFs of the DoP and CPD for four different sample areas are compared each other, and the threshold values for classifying SAR image data were determined by checking the cross-over points of the PDF fitting-lines of the different sample areas. The cross-over of the DoP PDF lines between the bare surface and the short vegetation field occurs at DoP=0.85, while the cross-over between the short vegetation field and the forest area at DoP=0.65. The determination of the cross-over value between the single-bounce dominated and the double-bounce dominated backscatter is not obvious. We chose the CPD value of $45^0$, comparing the PDF lines of the CPDs of the short vegetation field (single-bounce

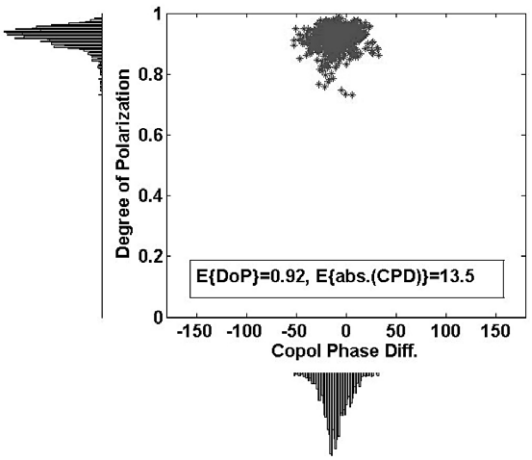


Fig. 1. DoP-CPD diagram with histograms for a bare soil area.

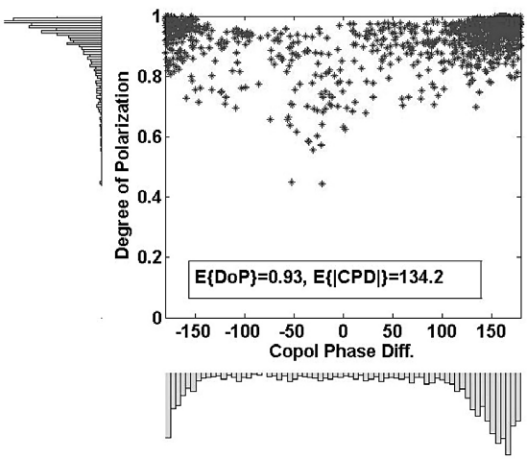


Fig. 2. DoP-CPD diagram with histograms for a village area.

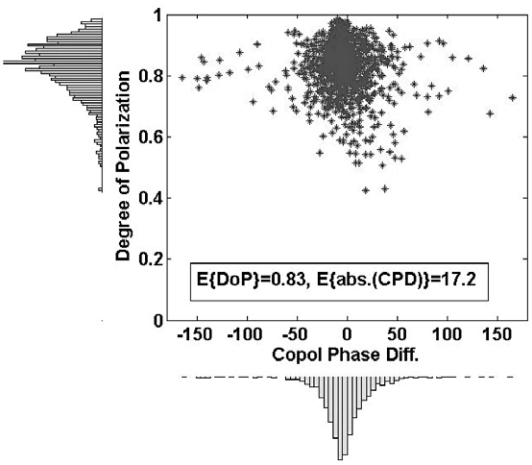


Fig. 3. DoP-CPD diagram with histograms for a short vegetation area.

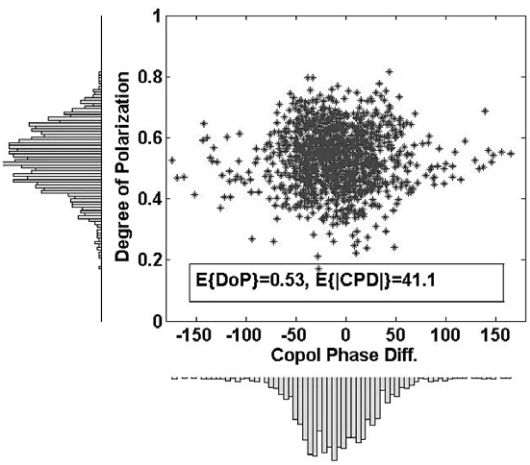


Fig. 4. DoP-CPD diagram with histograms for a forest area.

dominated) and the forest (mixed with single- and double-bounce scattering mechanism).

Based on the analysis of the DoP and CPD of the polarimetric image data, a new classification technique with six classification classes is proposed. For a distributed target, the DoP and CPD values of each pixel of a sample area are positioned in the DoP-CPD diagram with the vertical axis of the DoP and the horizontal axis of the CPD. The DoP-CPD diagram can also be used with the absolute values of the CPD because CPD is symmetry.

Fig. 5 shows the DoP-CPD diagram with six different zones, which have their own characteristics as described below.

- Zone I (high-DoP, low-|CPD| backscatter): Physical surfaces such as bare surfaces, water surfaces, sea-ice surfaces will fall in this category.
- Zone II (high-DoP, high-|CPD| backscatter): This zone corresponds to surface scattering with double bounce scattering events. Double-bounce-scattering structures on a bare surface such as a town or village with buildings will fall in this zone.
- Zone III (medium-DoP, low-|CPD| backscatter): The decreased DoP is due to a central statistical distribution of orientation angles of scattering particles. Such a zone would include scattering from relatively short-vegetated fields, such as farming fields.
- Zone IV (medium-DoP, high-|CPD| backscatter): This zone accounts for dihedral scattering with moderate DoP. This may occur with double-bounce backscatters beneath a sparse crown layer with randomly oriented leaves and branches.
- Zone V (low DoP, low-|CPD| backscatter): Volume scattering from a cloud of scatter particles is assumed to arise with DoP<0.65. This zone may include single-bounce dominated deciduous forests or a dense short vegetation fields.
- Zone VI (low DoP, high-|CPD| backscatter): Coniferous forest may have double-bounce scattering at a trunk layer with random scattering through a sparse crown layer, even though this scattering mechanism will depend on frequency.

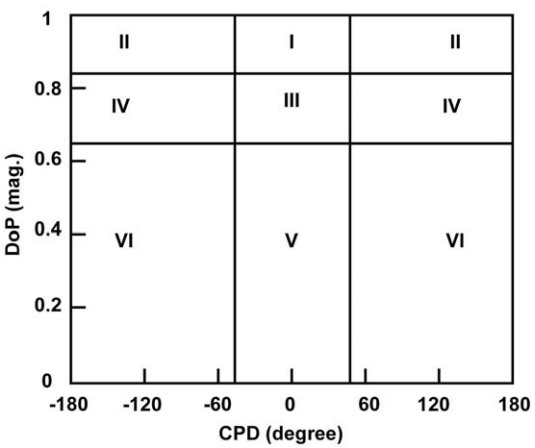

Fig. 5. Six zones of the DoP-CPD diagram.

## 4. Verification with SAR image data

The DoP-CPD diagrams are verified with the selected study areas. At first the new DoP-CPD classification technique has been applied to the JPL AirSAR images as shown in Table 1. Most pixels (1155 pixels among 1200 pixels; 96.3 %) of the bare surface are classified to the 'Zone I' of the DoP-CPD diagram. Most pixels (84.5%) of the town (village area) are classified to the 'Zone II' of the DoP-CPD diagram. For the short vegetation fields, the most pixels (88.6%) are classified to Zone I (28.0%) and Zone III (60.6), because the field is an orchard field with a very sparse tree-canopy. For the tall vegetation fields, 65% of the pixels are classified to Zone V,

while 23.8% of the pixels are classified to Zone VI as shown in Table 1, because the double bounce scattering may occur for a sparse forest area.

Polarimetric SAR image scenes for several sites in Korea could be obtained from the ALOS PALSAR (Phased Array L- band SAR) system in May, 2007. Table 2 shows the classification results for the PALSAR image data. The bare surfaces, which are mostly sea surfaces, could be excellently classified with the DoP-CPD Diagram technique. The accuracy of the classification for the sea surface was 96.4%. The accuracy of the DoP-CPD classification technique is also good for a forest area, a short vegetation area, and an urban area, as shown in Table 2. In this case, the short vegetation areas are mostly farming fields, and the urban area is a small town area.

Table 1. Accuracy of the classification technique for JPL AirSAR data

| Zone | Bare surface | | Village | | Short veg. | | Tall veg. | |
|---|---|---|---|---|---|---|---|---|
| | N | % | N | % | N | % | N | % |
| I | **1153** | **96.3** | 44 | 3.7 | 336 | 28.0 | 0 | 0.0 |
| II | 12 | 1.0 | **1014** | **84.5** | 19 | 1.6 | 0 | 0.0 |
| III | 33 | 2.8 | 35 | 2.9 | **727** | **60.6** | 97 | 8.1 |
| IV | 0 | 0.0 | 95 | 7.9 | 76 | 6.3 | 37 | 3.1 |
| V | 0 | 0.0 | 9 | 0.8 | 35 | 2.9 | **780** | **65.0** |
| VI | 0 | 0.0 | 3 | 0.3 | 7 | 0.6 | 286 | 23.8 |
| Total | 1200 | 100 | 1200 | 100 | 1200 | 100 | 1200 | 100 |

Table 2. Accuracy of the classification technique for PALSAR data

| Zone | Bare surface | | Forest | | Short veg. | | Urban area | |
|---|---|---|---|---|---|---|---|---|
| | N | % | N | % | N | % | N | % |
| I | **482** | **96.4** | 40 | 16.0 | 9 | 3.6 | 0 | 0.0 |
| II | 2 | 0.4 | **181** | **72.4** | 4 | 1.6 | 0 | 0.0 |
| III | 16 | 3.2 | 13 | 5.2 | **165** | **66.0** | 68 | 13.6 |
| IV | 0 | 0.0 | 16 | 6.4 | 39 | 15.6 | 21 | 4.2 |
| V | 0 | 0.0 | 0 | 0.0 | 16 | 6.4 | **377** | **75.4** |
| VI | 0 | 0.0 | 0 | 0.0 | 17 | 6.8 | 34 | 6.8 |
| Total | 500 | 100 | 250 | 100 | 250 | 100 | 500 | 100 |

## 5. Concluding Remarks

Based on the analysis for the DoP and CPD for various earth terrains using polarimetric SAR data, a new unsupervised classification technique for polarimetric SAR images has been proposed, which assigns each image pixel to the six different classes of the DoP-CPD diagram. The accuracy of the new classification technique was examined with polarimetric AirSAR and PALSAR image data.

## Acknowledgment

This work was supported by the Agency for Defense Development (ADD) through the Radio-wave Detection Research Center in Korea Advanced Institute of Science and Technology (KAIST).

## References

Boerner, W.-M, 2003. Recent advances in extra-wide-band polarimetry, interferometry and polarimetric interferometry in synthetic aperture remote sensing and its applications, *IEE Proceedings- Radar, Sonar and Navigation*, 150(3): 113-124.

Cloude, S. R. and E. Potter, 1996. A Review of Target Decomposition Theorems in Radar Polarimetry, *IEEE Trans. Geosci. Remote Sensing*, 34(2): 498-518.

Cloude, S. R. and E. Pottier, 1997. An Entropy Based Classification Scheme for Land Applications of Polarimetric SAR, *IEEE Trans. Geosci. Remote Sensing*, 35(1): 68-78.

Elies, P., B. Le Jeune, P. Olivard, J. Cariou, and J. Lotrian, 1997. The application of de-polarization analysis to polarimetric

characterization and classification of metallic and dielectric samples, *J. Phys. D :Appl. Phys*. 30.

Kong, J. A., A. A. Swartz, H. A. Yueh, L. M. Novak, and R. T. Shin, 1988. Identification of terraincover using the optimum polarimetric classifier, *Journal of Electromagnetic Waves and Applications*, 2: 171-194.

Lee, J. S., M. R. Grunes, and R. Kwok, 1994. Classification of multilook polarimetric SAR imagery based on complex Wishart distribution, *International Journal of Remote Sensing*, 15(11): 2299-2311.

Lee, J. S., and E. Pottier, 1990. Polarimetric Radar fImaging from Basics to Applications, CRC Press, Taylor & Francis Group, USA.

Rio, V. S., J. M. Mosquera, M. V. Isasa, and M. E. Lorenzo, 2006. Statistics of the degree of polarization, *IEEE Trans. Antennas Propag*., 54(7): 2173-2175.

Sinclair, G., 1950. The transmission and reception of elliptically polarized waves, *Proc. IRE*, pp.148-151,

Ulaby, F. T. and C. Elachi, 1990. *Radar Polarimetry for Geoscience Applications*, Artech House Remote Sensing Library.

Ulaby, F. T., K. Sarabandi, and A. Nashashibi, 1992. Statistical properties of the Mueller matrix of distributed targets, *IEE Proceedings-F*, 139(2): 136-146.

Van zyl, 1989. Unsupervised classificastion of scattering behavior using radar polarimetry data, *IEEE Trans. Geosci. Remote Sensing*., 27(1): 36-45.